Theoretical Study of the Mechanisms for the Alkoxyacetic Acids Decomposition

Luis R. Domingo,[†] María T. Picher,[†] Vicent S. Safont,[‡] Juan Andrés,*[,‡] and Gabriel Chuchani[§]

Departament de Química Orgànica, Universitat de València, Dr. Moliner 50, 46100 Burjassot, València, Spain, Departament de Ciències Experimentals. Universitat Jaume I, Box 224, 12080 Castelló, Spain, and Centro de Química, Instituto Venezolano de Investigaciones Científicas (IVIC), Apartado 21827, Caracas 1020-A, Venezuela

Received: October 27, 1998; In Final Form: February 25, 1999

The decomposition of three alkoxyacetic acids, methoxy, ethoxy, and isopropoxy acetic acids, has been studied by using ab initio calculations at the MP2/6-31G** level. Molecular mechanisms A and B have been characterized, corresponding to stepwise processes with formation of the corresponding alcohol and an α-lactone intermediate, achieved by the nucleophilic attack of either carbonylic or hydroxylic oxygen atoms followed by a ring opening process to yield formaldehyde and carbon monoxide. For ethoxyacetic and isopropoxyacetic acids, three additional reactive channels were thought to be possible on potential energy surface; mechanisms C and D are elimination processes to give the corresponding alkene and glycolic acid. The reaction pathways along mechanisms C and D take place by the transfer of a β-hydrogen atom, with respect to the ether group, from the terminal methyl group to the hydroxylic or the alkoxylic oxygen atoms, respectively. The glycolic acid formed in the first step is then submitted to decomposition by water elimination and α-lactone intermediate formation. A final ring opening process yields formaldehyde and carbon monoxide. Molecular mechanism E is associated with a fragmentation process along a concerted one-step with concomitant formation of the corresponding alquene, formaldehyde, water, and carbon monoxide. The decomposition process is energetically favorable along the mechanism A, and the calculated rate coefficients agree with experimental data.

Introduction

The kinetics of the gas-phase decomposition of several carboxylic acid derivatives have been experimentally studied by Chuchani and co-workers,[1−5] in particular, the gas-phase decomposition of several alkoxyacetic acids, $ROCH_2COOH$, to give mainly formaldehyde, carbon monoxide, and the corresponding alcohol has been monitored and the results prove the reaction to be homogeneous and unimolecular and that it obeys a first-order rate law.[4] The rate coefficients in the temperature range 350.4−410.8 °C at a pressure range of 57−261.5 Torr can be expressed by the following Arrhenius-type equations:

$$ROCH_2COOH \rightarrow ROH + CH_2O + CO \qquad (1)$$

methoxyacetic acid (R = $-CH_3$), **I**,

$$\log k_{obs}(s^{-1}) = (12.10 \pm 0.22) - (193.3 \pm 2.8)\ \text{kJ mol}^{-1}\ (2.303RT)^{-1} \qquad (2)$$

ethoxyacetic acid (R = $-CH_2CH_3$), **II**,

$$\log k_{obs}(s^{-1}) = (12.76 \pm 0.29) - (199.6 \pm 3.7)\ \text{kJ mol}^{-1}\ (2.303RT)^{-1} \qquad (3)$$

isopropoxyacetic acid (R = $-CH(CH_3)_2$), **III**,

$$\log k_{obs}(s^{-1}) = (12.40 \pm 0.32) - (193.7 \pm 3.9)\ \text{kJ mol}^{-1}\ (2.303RT)^{-1} \qquad (4)$$

However, the mechanism by which these compounds decompose is still poorly defined at the atomic level so that the relationship between the mechanisms and the rate coefficients is not clear. Information obtained from kinetic studies can be augmented by geometry and energy considerations based on quantum mechanical calculations. Although the absolute accuracy of calculated reaction rates is still limited, calculations are able to provide reasonable values of rate coefficients. Quantum mechanical techniques can be used to obtain the potential energy surface (PES) associated with a chemical reaction.[6,7] These PESs are devices designed to characterize stationary points representing chemical species relevant to different kinetic mechanisms, and their analysis provides molecular geometries and vibrational frequencies for reactants (R), products (P), intermediates (IN), and transition structures (TS). From these data, barrier heights and rate coefficients for the reaction pathways connecting the reactants with the products via the corresponding transition structures can be calculated with practical accuracy. The transition state theory (TST)[8,9] was devised to facilitate the interpretation of rate coefficients and is used almost universally, albeit loosely, by chemists interested in reaction mechanisms. Other theories have been developed to calculate the rate coefficients for chemical processes,[10] such as the RRKM[11,12] or the VTST[13,14] however, the mechanism of a given chemical reaction can be described by the transition structure associated with the chemical interconversion step in the sense proposed by Tapia and Andrés.[15,16] We have selected this method to calculate the kinetic parameters in the present study.

* To whom correspondence should be addressed.
[†] Universitat de València.
[‡] Universitat Jaume I.
[§] Instituto Venezolano de Investigaciones Científicas.

10.1021/jp984225w CCC: $18.00 © 1999 American Chemical Society
Published on Web 04/30/1999

SCHEME 1

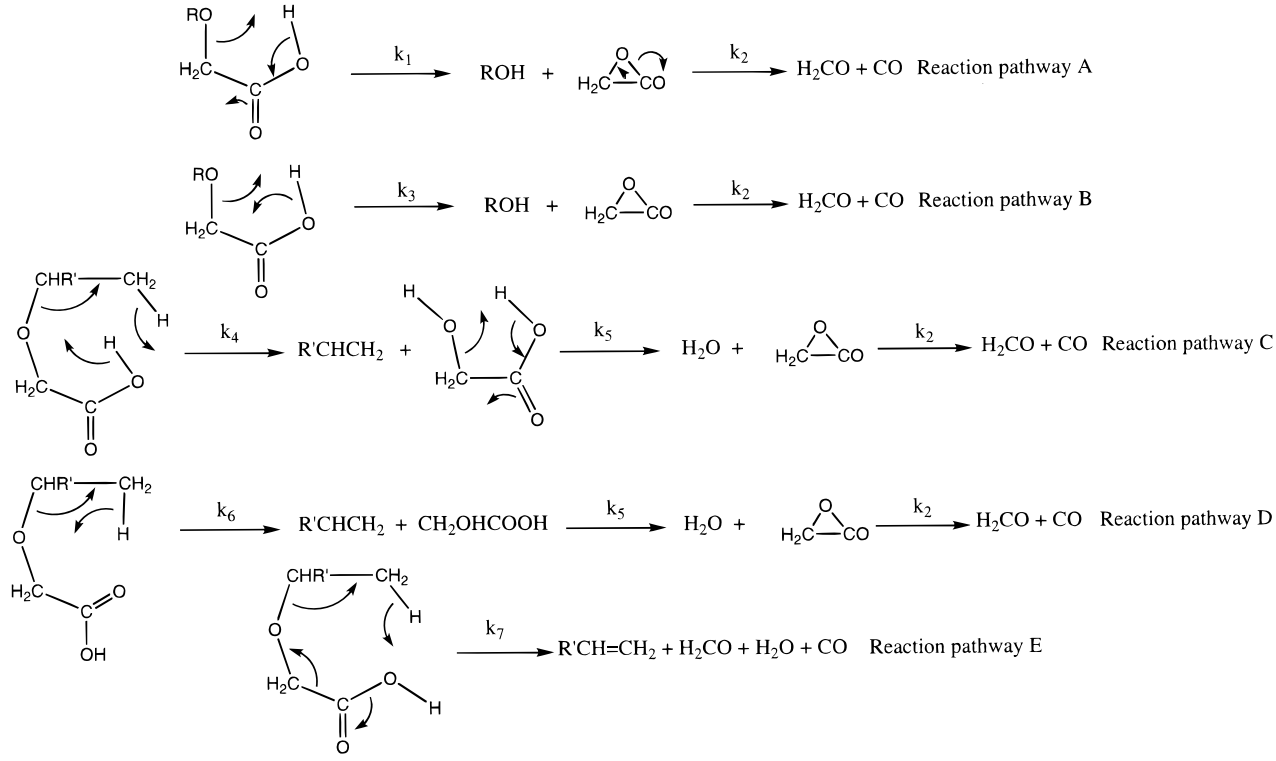

Note: For **I** (R=-CH_3), only reaction pathways A and B are possible
For **II** (R=-CH_2CH_3; R'=H) and **III** (R=-$CH(CH_3)_2$; R'=CH_3), the five reaction pathways have been studied

Recently, we have reported quantum mechanical calculations on 2-chloropropionic acid,[17] glycolic, lactic, and 2-hydroxyisobutiric acid,[18] and mandelic acid[19] decompositions in order to explain the experimental behavior of these systems. As a part of a project designed to characterize and investigate more complex systems, this paper describes the characterization of the **I**, **II**, and **III** decomposition processes, with the main objective being the analysis of the reactive PES, the description of the nature of the mechanism, and the rationalization of the experimental observations.

Computational Method and Model

Calculations at full MP2 level of theory with the 6-31G** basis set[20] have been performed with the GAUSSIAN94[21] program. Recent studies on the related systems have shown that this level of theoretical approximation is a reasonable choice and that further enhancements, like an MCSCF approach with CASSCF treatment, yields very similar results with respect to structural and kinetic parameters[17] and reaction profiles.[18,19]

The Berny analytical gradient optimization routines[22,23] were used for optimization. The requested convergence on the density matrix was 10^{-9} au, the threshold value of maximum displacement was 0.0018 Å, and that of maximum force was 0.00045 hartree/b. The nature of each stationary point was established by calculating and diagonalizing the Hessian matrix (force constant matrix). The transition structures were characterized by means of a normal-mode analysis, and the unique imaginary frequency associated with the transition vector,[24] i.e., the eigenvector associated with the unique negative eigenvalue of the force constants matrix, has been characterized. The intrinsic reaction coordinate (IRC)[25] path was traced in order to check and obtain the energy profiles connecting each transition structure to the two associated minima of the proposed mechanism by using the second-order González−Schlegel integration method.[26,27]

Each stationary structure was characterized as a minimum or a saddle point of index 1 by a frequency calculation. This frequency calculation also provides thermodynamic quantities such as zero-point vibrational energy (ZPVE), temperature corrections ($E(T)$), and the absolute entropy ($S(T)$),[28] and consequently, the rate coefficient can be estimated. Temperature corrections and absolute entropies were obtained, assuming ideal gas behavior, from the harmonic frequencies and moments of inertia by standard methods.[29] A temperature of 653 K (379.8 °C), similar to the experimental data, was used, while a standard pressure of 1 atm was taken in the calculations.

Results and Discussion

An extensive exploration of the PES renders that five reaction pathways may be associated with the decomposition process of $ROCH_2COOH$, and they are depicted in Scheme 1.

Within the mechanism A, the formation of the α-lactone intermediate and the corresponding alcohol product, ROH, is achieved, via the **TS1**, by the nucleophilic attack of the carbonylic oxygen atom on the α-carbon of the corresponding alkoxyacetic acid. A hydrogen atom transfer from the hydroxylic oxygen to the alkoxylic oxygen accompanies this attack.

The formation of the α-lactone intermediate and alcohol product is also achieved in the mechanism B by the nucleophilic attack of the hydroxylic oxygen atom on the α-carbon of the corresponding alkoxyacetic acid, through **TS3**. A hydrogen atom transfer from the hydroxylic oxygen to the alkoxylic oxygen also accompanies this attack. Both reaction pathways A and B have a common second step, associated with the ring cleavage

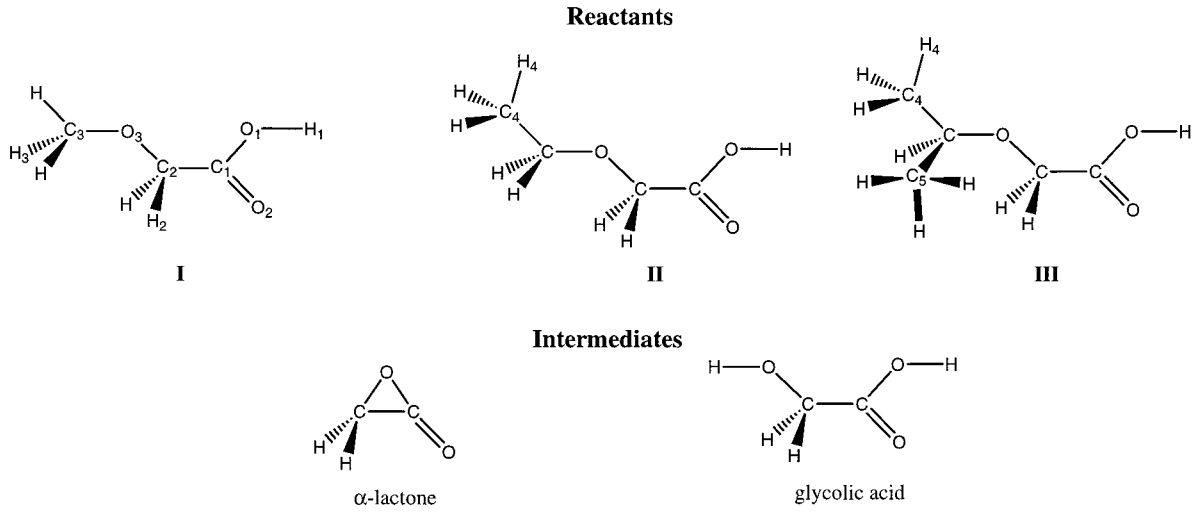

Figure 1. Stationary points, reactants, and intermediates for the different decomposition processes. The atom numbering is also indicated.

of the α-lactone intermediate via **TS2**, yielding formaldehyde and carbon monoxide.

Mechanism C is a three-step process, beginning with an elimination reaction, by the transfer of a β-hydrogen atom, with respect to the ether group, from the terminal methyl group to the hydroxylic oxygen atom. The corresponding **TS4** shows (see below) that this hydrogen transfer is coupled with another hydrogen shift from the hydroxylic to the alkoxylic oxygen, thus giving a place to the corresponding alkene ($R' = -H$ for **II**, $R' = -CH_3$ for **III**) product and the glycolic acid intermediate. The second step is a dehydration process, through **TS5**, with formation of the α-lactone intermediate. The final step is associated with the ring cleavage. A recent theoretical study on the decomposition of glycolic acid was already reported[18] in which it was shown that three possible mechanisms can lead to its final decomposition products, water, carbon monoxide, and formaldehyde. The results obtained demonstrate that the mechanism through the α-lactone intermediate is the most favorable; therefore, this is the mechanism considered here from glycolic acid.

Mechanism D is similar to mechanism C, but there is only one hydrogen transfer process along the first step, which takes place from the terminal methyl group to the alkoxy oxygen atom, via **TS6**, with formation of the alkene product and the glycolic acid intermediate. Both mechanisms C and D are not possible for **I**.

The mechanism E is associated with a fragmentation process along a concerted one-step process, to give the corresponding alkene, formaldehyde, water, and carbon monoxide, through **TS7**. This mechanism is not possible for **I**. An alternative one-step process, to give the alkene, water, and the α-lactone intermediate, was also investigated, but the α-lactone moiety is found to be very strained and the ring cleavage is coupled with the alkene production; **TS7** is found again.

Assuming the irreversible nature of the decomposition processes, the apparent first-order rate coefficients would be obtained by means of

$$k_{ap} = k_1 + k_3 + k_4 + k_6 + k_7 \qquad (5)$$

Geometries and Transition Vectors. In Figure 1, the reactants (**I**, **II**, and **III**) and intermediates, α-lactone and glycolic acid, for the decomposition processes are sketched. The corresponding products are methanol, ethanol, and 2-propanol; formaldehyde and carbon monoxide; ethene, propene, and water. The atom numbering is also indicated in Figure 1. In Figure 2 all calculated transition structures are depicted, parts a, b, and c for the **I**, **II**, and **III** decompositions, respectively. The optimized geometrical parameters for all stationary points found are available from the authors on request.

As Supporting Information (Table 1as−es), the imaginary frequency, the Hessian unique negative eigenvalue, and the main transition vector components and corresponding geometric parameters are reported for the transition structures. An analysis and comparison of the results show a remarkable invariance concerning geometric parameters, index, and transition vector amplitudes. The geometric parameters and transition vector components for **TS2** and **TS5** are not reported. They can be found in our recent report on the decomposition of glycolic, lactic, and 2-hydroxyisobutyric acids.[18]

For **TS1** (Table 1as of the Supporting Information), the geometric parameters reported show long C2−O3 and O1−H1 distances, as expected for bonds that are being broken at the transition structure. In addition, the O2−C2 distance (a bond being formed) is still long at **TS1**, indicating a reactant-like character with respect to this variable. On the other hand, the dominant transition vector components correspond to the C2−O3 and O2−C2 bond distances in the three model systems, in antiphase as expected. The O1−C1−C2 bond angle has an important participation to the transition vector, in antiphase with the O2−C2 distance, indicating that a reduction of the distance is coupled with an opening of this angle. The **TS1** can be described as a bicyclic structure, with the H1 at one of the edges of a distorted five-membered ring, shifting from O1 to O3. The second ring is three-membered, with O2 approaching C2 to close the propiolactone ring. A perusal of the transition vector amplitudes shows that the **TS1** is well associated to the expected atom motions. The imaginary frequency values are in the range of 554−564i cm^{-1}, remarkably invariant as well, indicating that these stationary points are associated with the heavy atom motions. Normal mode animation (using GaussView[30]) of **TS1** shows the dominance of the C2 fluctuation, the C2−O3 distance fluctuates in antiphase with the O2−C2 and the O1−H1 distances. The change in dihedral angle of H2 and H2′ accompanies the fluctuations, which are fully localized to this atom framework and are remarkably invariant to the system size.

For **TS3** (Table 1bs of the Supporting Information) a much longer C2−O3 distance with respect to the **TS1** is obtained, thus indicating that in this case the alcohol elimination is more

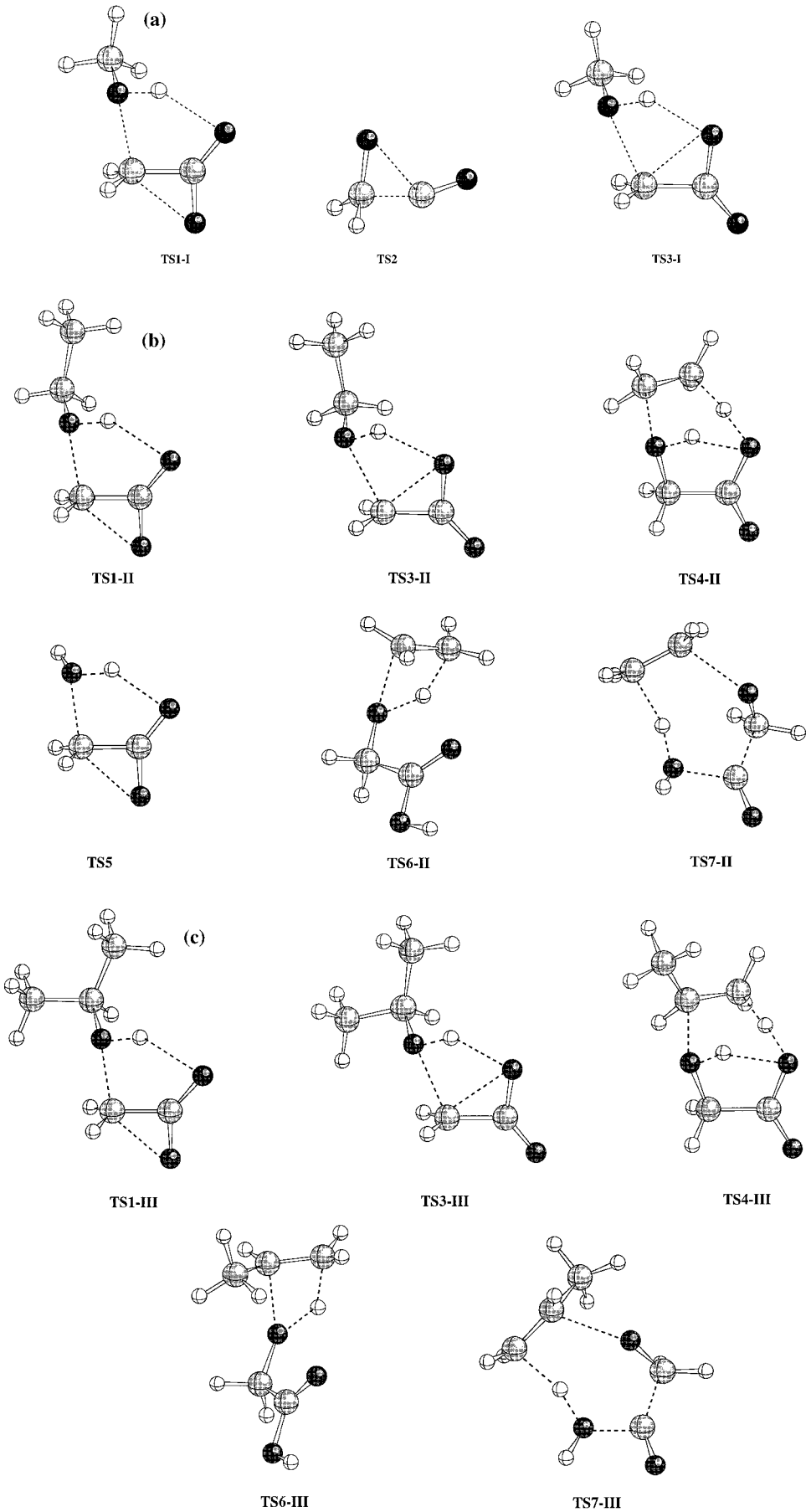

Figure 2. (a) Transition structures **TS1**−**I**, **TS2**, and **TS3**−**I**. Note that **TS2** is the same for **I**, **II**, and **III**. (b) Transition structures **TS1**−**II**, **TS3**−**II**, **TS4**−**II**, **TS5**, **TS6**−**II**, and **TS7**−**II**. Note that **TS5** is the same for **II** and **III**. (c) Transition structures **TS1**−**III**, **TS3**−**III**, **TS4**−**III**, **TS6**−**III**, and **TS7**−**III**.

TABLE 1: Absolute Electronic Energies (*E*, au), Zero-Point Energies and Temperature Corrections (*Z*, au) and Entropies (*S*, J mol^{-1} K^{-1}) of the Stationary Points Found, and Relative Enthalpies ($\Delta H^{\ddagger}$, kJ mol^{-1}) and Relative Entropies ($\Delta S^{\ddagger}$, J mol^{-1} K^{-1}) to the Corresponding Reactants of the Indicated Transition Structures[a]

	E	*Z*	*S*	$\Delta H^{\ddagger}$	$\Delta S^{\ddagger}$	*k*
I	−342.666 240	0.122 033	448.92			
TS1−I	−342.583 669	0.118 820	441.05	208.35	−7.87	$k_1 = 1.14 \times 10^{-4}$
TS3−I	−342.551 578	0.118 270	451.88	291.17	2.96	$k_3 = 9.95 \times 10^{-11}$
methanol	−115.387 563	0.060 998	270.62			
lactone	−227.206 258	0.051 614	318.52			
TS2	−227.151 796	0.048 292	320.16	134.27	1.64	$k_2 = 301.44$
H_2CO	−114.191 016	0.034 808	250.60			
CO	−113.028 180	0.010 101	221.07			
II	−381.859 121	0.156 804	505.28			
TS1−II	−381.777 125	0.153 619	494.84	206.92	−10.44	$k_1 = 1.09 \times 10^{-4}$
TS3−II	−381.744 717	0.153 052	505.46	290.52	0.18	$k_3 = 8.03 \times 10^{-11}$
ethanol	−154.582 081	0.097 790	335.45			
TS4−II	−381.749 422	0.149 143	470.47	267.90	−34.81	$k_4 = 7.69 \times 10^{-11}$
TS6−II	−381.743 242	0.148 814	495.97	283.26	−9.31	$k_6 = 9.75 \times 10^{-11}$
ethene	−78.327 231	0.062 150	274.13			
glycolic	−303.497 181	0.085 448	367.62			
TS5	−303.410 689	0.083 787	381.78	222.72	14.16	$k_5 = 1.14 \times 10^{-4}$
H_2O	−76.222 449	0.028 310	215.70			
TS7−II	−381.698 892	0.148 267	497.93	398.27	−7.35	$k_7 = 7.80 \times 10^{-20}$
III	−421.052 396	0.191 371	545.90			
TS1−III	−420.971 855	0.188 084	543.61	202.83	−2.29	$k_1 = 6.16 \times 10^{-4}$
TS3−III	−420.938 790	0.187 470	555.82	288.03	9.92	$k_3 = 4.09 \times 10^{-10}$
i-propanol	−193.776 162	0.132 301	386.82			
TS4−III	−420.946 993	0.183 693	525.55	256.58	−20.35	$k_4 = 3.52 \times 10^{-9}$
TS6−III	−420.939 457	0.183 398	548.15	275.59	2.25	$k_6 = 1.61 \times 10^{-9}$
propene	−117.519 080	0.096 950	331.18			
TS7−III	−420.894 704	0.182 437	554.04	390.56	8.14	$k_7 = 2.08 \times 10^{-18}$

[a] It must be noted that the reactants for TS2 and TS5 are, respectively the lactone and the glycolic acid. Theoretically calculated (at 653 k) first-order rate coefficients (*k*, s^{-1}). The apparent first-order rate coefficients obtained from eq 5 coincide with the k_1 values. The experimental intervals for the observed rate coefficients at 653 K are 1.21×10^{-3} to 1.57×10^{-4} s^{-1} for **I**, 2.41×10^{-3} to 1.63×10^{-4} s^{-1} for **II**, and 3.47×10^{-3} to 1.89×10^{-4} s^{-1} for **III**.

advanced than in the preceding case. The **TS3** has a distorted five-membered ring shape, with O1 approaching C2 to close the propiolactone ring. On the other hand, there are two transition vector dominant components, the C2−O3 and O1−C2 bond distances, in antiphase to each other. The C2−C1−O2 component also has an important participation in the transition vector, in phase with the C2−O3 bond distance; the corresponding angle opens as the alcohol is eliminated and the O1 atom closes the lactone ring. The closure of the lactone ring is then described as coupled with the leaving of the alcohol moiety and the O2 motion. The imaginary frequency values are in the range of 585−595i cm^{-1}, indicating that the **TS3** is associated with the heavy atom motions. Normal mode animation of **TS3** shows a concerted motion of the O1, C1, C2, O3, and H1 atoms, with a small bending of the O2 atom. The O1 and C2 atoms approach each other, while H1 and O3 move away from it (respectively, from O1 and C2). It is interesting that the O1−H1 distance shows only very small fluctuation; the hydroxylic O−H bond is almost formed at **TS3**.

For **TS4** (Table 1cs of the Supporting Information), a slightly short C3−C4 bond distance indicates the incipient double bond character; meanwhile, the large values of O3−C3, O1−H1, and C4−H4 distances describe the breaking of these bonds at the transition structure. The **TS4** can be described as a bicyclic structure, with the H1 atom shifting from O1 to O3 and the H4 atom moving from C4 to O1 (see parts b and c of Figure 2). The dominant transition vector components correspond to the C4−H4 bond distance, in phase with the O3−C3 bond distance, describing the leaving of the corresponding alkene. The imaginary frequency values are in the range 1293−1423i cm^{-1}, indicating that the **TS4** is strongly associated with the hydrogen motions. In fact, normal mode animation of **TS4** shows the dominance of H4 fluctuation between C4 and O1, with a coupled motion of H1 (from O1 to O3, as indicated) and a slight stretching of the C1−O1 and O3−C3 bonds. The alkene moeity shows a slight motion from a pyramidalized to a planar conformation.

An analysis of the results for **TS6** (Table 1ds of the Supporting Information) shows that the process is associated with a typical 1,2 elimination with C3−C4 double bond formation. **TS6** can be described as a four-membered ring, with H4 moving from C4 to O3, yielding the alkene with concomitant glycolic acid formation (see parts b and c of Figure 2). The leading transition vector component is associated with the O3−H4 bond (which is being formed), in antiphase with the O3−C3 bond length (which is being broken). The imaginary frequency values are in the range 1906−1988 i cm^{-1}, showing that the **TS6** is mainly associated with the H4 atom motion. Normal mode animation of **TS6** shows that the fluctuation is almost only localized to the H4 motion; only small fluctuations of the alkene moiety (to a more planar conformation) accompany it.

For **TS7** (Table 1es of the Supporting Information), large values for the O3−C3, O1−C1, and C4−H4 distances are found, while the C3−C4 distance is changing from single to double bond. **TS7** can be described as a distorted seven-membered ring (see parts b and c of Figure 2), with coupled O3−C3, C1−C2, O1−C1, and C4−H4 bond breaking processes and O1−H4 bond formation. The main transition vector components correspond to the O3−C3, C4−H4, and O1−C1 bond distances in phase; these components are in antiphase with the C3−C4 bond distance. The imaginary frequency values are in the range 669−764i cm^{-1}, indicating that the **TS7** is mainly associated with the heavy atom motions and with the H4 atom motion as well. The normal mode animation of **TS7** shows a concerted process where the dominant fluctuation is the H4 shift

from C4 to O1, with strong flapping of the alkene moiety, less strong motion of O3 and the O1−H1 and C1−O2 fragments, and very small fluctuation of the C1−C2 distance.

Energetics and Kinetic Parameters. Free energy profiles for the decomposition processes of the three systems are presented in parts a, b, and c of Figure 3 for **I**, **II**, and **III**, respectively. From the energetic data, a complete analysis of the activation parameters has been carried out, and the results are presented in Table 1.

At first sight, it appears clearly that the decompositions are spontaneous processes that will take place through the reaction pathway A almost exclusively. The associated activation enthalpies of the A first step are much lower than the activation enthalpies associated to the first step of the rest of reaction pathways herein studied. Then the apparent rate coefficients coincide with the first-order rate coefficient associated with the first step of the A mechanism. This observation excludes reaction pathway B to be kinetically significant, and the same can be assessed for reaction pathway E for **II** and **III** (see Table 1). However, it was experimentally observed that there was little amount of propene formation in the decomposition of **III**.[4] This may be achieved either by means of reaction mechanisms C and D or by direct dehydration within the experimental conditions of 2-propanol. We have explored this latter possibility, and a very high activation enthalpy of 291.88 kJ mol^{-1} was found, as compared to the values for **TS4**−**III** and **TS6**−**III** reported in Table 1. Furthermore, a theoretical first-order rate coefficient of 7.16×10^{-11} s^{-1} is calculated for the direct 2-propanol dehydration, a process slower than either reaction pathways C ($k_4 = 1.61 \times 10^{-9}$ s^{-1}) or D ($k_6 = 3.52 \times 10^{-9}$ s^{-1}). Therefore, the direct 2-propanol dehydration can be excluded in the experimental conditions.

For the **II** system, mechanisms C and D would open the possibility for an ethene formation. However, ethene was not found experimentally as a product for the **II** decomposition. The lack of ethene formation can be justified by the higher activation free energy needed (289 or 291 kcal/mol for **TS6**−**II** or **TS4**−**II**, respectively; see Figure 3b) as compared with the activation free energy to the transition structure that opens the pathway for propene formation (270 or 274 kcal/mol for **TS4**−**III** or **TS6**−**III**, respectively; see Figure 3c).

A comparison between the calculated and experimental values for the rate coefficients shows a very good agreement. According to the experimental data, the decomposition rate coefficient at 653 K is in the range of 1.21×10^{-3} to 1.57×10^{-4} s^{-1} for **I**, 2.41×10^{-3} to 1.63×10^{-4} s^{-1} for **II**, and 3.47×10^{-3} to 1.89×10^{-4} s^{-1} for **III**, while the computed values are 1.14×10^{-4} s^{-1}, 1.09×10^{-4} s^{-1}, and 6.16×10^{-4} s^{-1} for **I**, **II**, and **III**, respectively.

As can be seen, the system size does not affect very much the rate coefficient value. This experimental result is theoretically reproduced and can be explained because the O2 attack on C2 prompts for an alkoxy group elimination (see **TS1**−**I**, **TS1**−**II**, and **TS1**−**III** in parts a, b, and c of Figure 2), assisted by the hydrogen shift from O1 to O3. Methoxy, ethoxy, and isopropoxy groups behave very similarly as leaving groups, and then there is no reason for significant differences in the rate coefficient values.

Bond Orders. The bond order (B) concept can be used to obtain a deeper analysis of the extent of bond formation or bond breaking along a reaction pathway.[31−33] To follow the nature of the decomposition process, the Wiberg bond indices[34] have been computed by using the natural bond orbital (NBO)[35,36] analysis as implemented in Gaussian94.[21] There are several breaking−forming bond processes along the fragmentation processes and the global nature of the decomposition reaction can be monitored by means of the synchronicity (Sy) concept proposed by Moyano et al.,[37] using the following expression:

$$\mathrm{Sy} = 1 - \frac{\sum_{i=1}^{n} \frac{|\partial B_i - \partial B_{\mathrm{av}}|}{\partial B_{\mathrm{av}}}}{2n - 2} \tag{6}$$

In eq 6 n is the number of bonds directly involved in the reaction, and the relative variation of the bond index is obtained from

$$\partial B_i = \frac{B_i^{\mathrm{TS}} - B_i^{\mathrm{R}}}{B_i^{\mathrm{P}} - B_i^{\mathrm{R}}} \tag{7}$$

where the superscripts TS, R, and P refer to the transition structure, reactant, and product, respectively. The average value ∂B_{av} is therefore

$$\partial B_{\mathrm{av}} = n^{-1} \sum_{i=1}^{n} \partial B_i \tag{8}$$

Synchronicities calculated from expression 6 and the Wiberg bond indices[34] of the breaking/making bond processes are reported in Table 2. The percentage of evolution of the bond order through the chemical step has been calculated by means of

$$\%\ \mathrm{EV} = \frac{B_i^{\mathrm{TS}} - B_i^{\mathrm{R}}}{B_i^{\mathrm{P}} - B_i^{\mathrm{R}}} \times 100 \tag{9}$$

The results are also included in Table 2.

For **TS1** (Table 2) it can be seen that the H1 displacement from O1 to O3 is very advanced; the O1−H1 bond is almost broken (around 93%) while the O3−H1 bond is almost formed (around 82%). Furthermore, the breaking of the original C2−O3 bond is also advanced, and the same can be observed for the double bond formation at the C1−O1 bond. However, the O2 assistance is late; the C2−O2 bond forming is only at a 35%. Then, the enlargement of the C2−O3 bond with initial migration of the H1 atom can be seen as the driving force for the decomposition process. The invariance of the results to the system size is remarkable, and the synchronicity value of 0.87 shows that the first step of the reaction pathway A can be described as concerted but slightly asynchronous. The second step of the A and B reaction pathways are not analyzed here; they have been studied elsewhere.[18]

For **TS3** (Table 2), again the H1 migration from O1 to O3 is very advanced, 93% evolution of the O1−H1 bond breaking and 83% evolution of the O3−H1 bond formation. As in **TS1**, the oxygen assistance (in this case, the O1 assistance) to the process is late; the C2−O1 bond formation has advanced less than 30%, while the C2−O3 cleavage has been produced to a great extent. The results are invariant to the system size, and the synchronicity value of 0.81 shows that the first step of reaction pathway B can be described as asynchronous concerted.

The **TS4** (Table 2) is characterized by a double hydrogen shift, the H1 passage from O1 to O3, which is very advanced at the transition structure, and the H4 migration from C4 to O1, which, on the contrary, is late. In this case, it is the C3−O3 bond which is broken, prompting for the corresponding

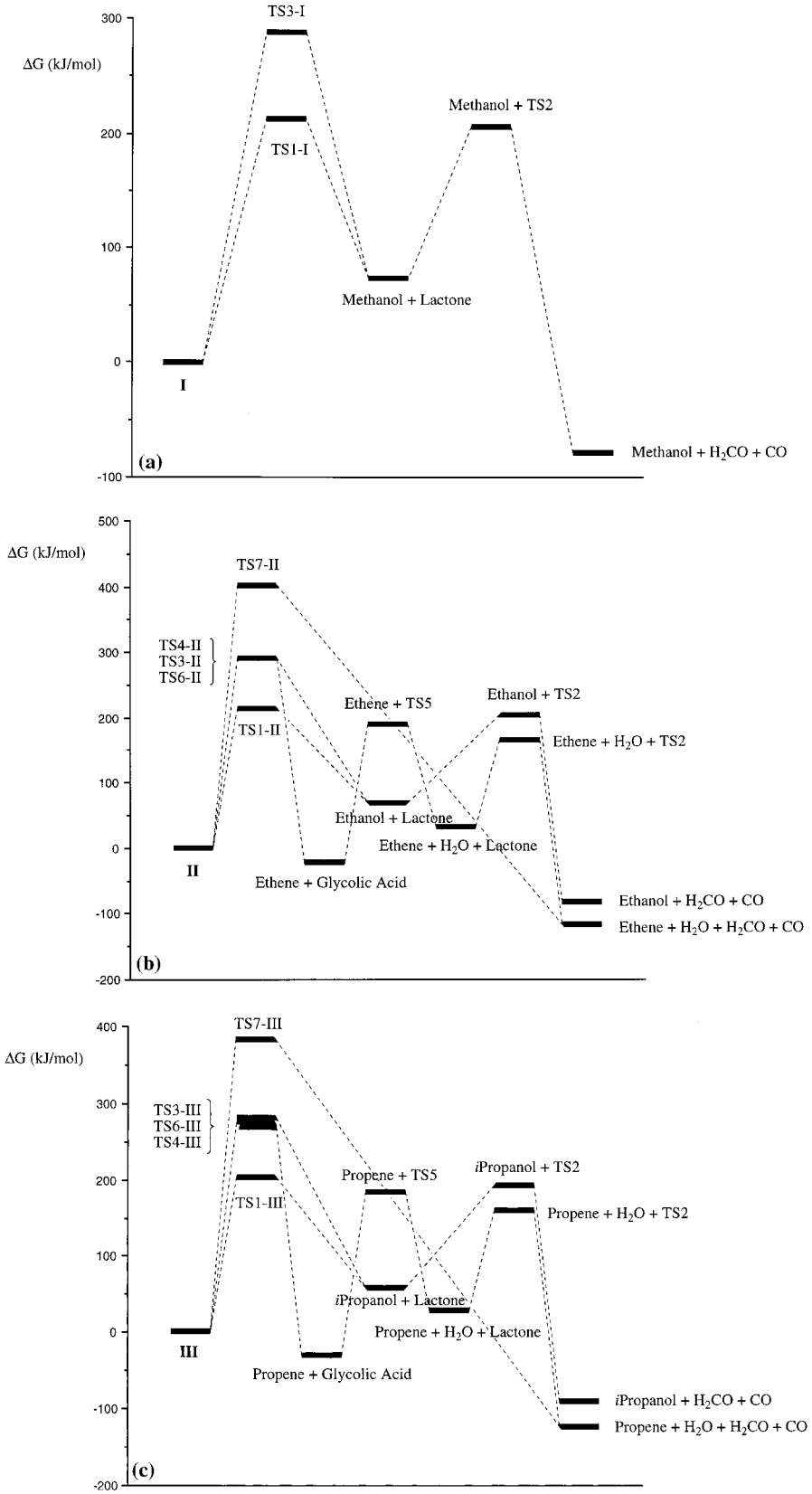

Figure 3. Free energy profiles at 653 K for the (a) **I**, (b) **II**, and (c) **III** decomposition process. (a) Relative free energy values (to reactant **I**, in kJ mol^{-1}) of the stationary points found are as follows: **TS1**−**I**, 213.5; **TS3**−**I**, 289.2; methanol + lactone, 73.8; methanol + **TS2**, 207.0; methanol + H_2CO + CO, −77.7. (b) Relative free energy values (to reactant **II**, in kJ mol^{-1}) of the stationary points found are as follows: **TS1**−**II**, 213.7; **TS3**−**II**, 290.4; ethanol + lactone; 69.3; ethanol + **TS2**, 202.5; ethanol + H_2CO + CO, −82.3; **TS4**−**II**, 290.6; **TS6**−**II**, 289.3; ethene + glycolic acid, −22.2; ethene + **TS5**, 191.3; ethene + H_2O + lactone, 34.3; ethene + H_2O + **TS2**, 167.5; **TS7**−**II**, 403.1; Ethene + H_2O + H_2CO + CO, −117.3. (c) Relative free energy values (to reactant **III**, in kJ mol^{-1}) of the stationary points found are as follows: **TS1**−**III**, 204.3; **TS3**−**III**, 281.6; *i*-propanol + lactone; 60.0; *i*-propanol + **TS2**, 193.2; *i*-propanol + H_2CO + CO, −91.5; **TS4**−**III**, 269.9; **TS6**−**III**, 274.1; propene + glycolic acid, −28.5; propene + **TS5**, 184.9; propene + H_2O + lactone, 28.0; propene + H_2O + **TS2**, 161.2; **TS7**−**III**, 385.2; propene + H_2O + H_2CO + CO, −123.6.

TABLE 2: Wiberg Bond Indices (B_i), Percentage of Evolution through the Chemical Process (%Ev) of the Bond Indices at the Transition States, Calculated by Means of Eq 9, and Synchronicity Values (Sy) Obtained from Eq 6

		C1−O1	C2−O3	C2−O2	O1−H1	O3−H1	C1−O2
TS1−I	B_i^R	1.022	0.894	0.047	0.674	0.020	1.724
	B_i^{TS}	1.523	0.292	0.320	0.048	0.622	1.339
	% Ev	66.2	67.3	35.0	92.9	82.4	53.3
				Sy = 0.87			
TS1−II	B_i^R	1.021	0.894	0.047	0.674	0.021	1.723
	B_i^{TS}	1.525	0.288	0.325	0.046	0.627	1.335
	% Ev	66.5	67.8	35.6	93.2	82.9	53.8
				Sy = 0.87			
TS1−III	B_i^R	1.023	0.893	0.047	0.670	0.025	1.722
	B_i^{TS}	1.526	0.288	0.327	0.046	0.627	1.333
	% Ev	66.5	67.7	35.9	93.1	82.6	54.0
				Sy = 0.87			

		C2−O3	C2−O1	O1−H1	O3−H1
TS3−I	B_i^R	0.894	0.020	0.674	0.020
	B_i^{TS}	0.232	0.258	0.042	0.629
	% Ev	74.0	29.5	93.8	83.3
			Sy = 0.81		
TS3−II	B_i^R	0.894	0.020	0.674	0.021
	B_i^{TS}	0.231	0.259	0.043	0.630
	% Ev	74.2	29.6	93.6	83.3
			Sy = 0.81		
TS3−III	B_i^R	0.893	0.020	0.670	0.025
	B_i^{TS}	0.230	0.257	0.046	0.626
	% Ev	74.2	29.4	93.1	82.4
			Sy = 0.81		

		O1−H1	O3−H1	C3−O3	C3−C4	C4−H4	O1−H4
TS4−II	B_i^R	0.674	0.021	0.858	1.030	0.934	0.000
	B_i^{TS}	0.056	0.613	0.338	1.312	0.481	0.256
	% Ev	93.9	86.5	60.6	28.1	48.5	36.7
				Sy = 0.78			
TS4−III	B_i^R	0.670	0.025	0.842	1.014	0.937	0.000
	B_i^{TS}	0.059	0.616	0.278	1.287	0.507	0.235
	% Ev	93.4	86.9	67.0	28.1	45.9	33.7
				Sy = 0.76			

		C3−O3	C3−C4	C4−H4	O4−H4
TS6−II	B_i^R	0.858	1.030	0.934	0.008
	B_i^{TS}	0.353	1.357	0.413	0.267
	% Ev	58.9	32.6	55.8	37.2
			Sy = 0.84		
TS6−III	B_i^R	0.842	1.014	0.937	0.001
	B_i^{TS}	0.311	1.331	0.423	0.252
	% Ev	63.1	32.6	54.9	35.7
			Sy = 0.82		

		C1−O1	O1−H4	C4−H4	C3−C4	C3−O3	C2−O3	C1−C2
TS7−II	B_i^R	1.021	0.000	0.934	1.030	0.858	0.894	0.976
	B_i^{TS}	0.594	0.406	0.211	1.625	0.184	1.045	0.976
	% Ev	41.8	53.1	77.4	59.3	78.6	15.5	0.0
					Sy = 0.70			
TS7−III	B_i^R	1.023	0.000	0.937	1.014	0.842	0.893	0.975
	B_i^{TS}	0.636	0.365	0.246	1.584	0.131	1.054	0.975
	% Ev	37.8	47.8	73.7	58.7	84.4	16.5	0.0
					Sy = 0.70			

alkene formation. However, the C3−C4 double bond formation is very late, thus indicating a very asynchronous process. This is also reflected by a lower synchronicity value than the preceding cases, although the concerted character is not lost, as indicated by the fact that only one transition structure describes the fragmentation. The second and third steps of the reaction pathways C and D have been studied in a related work.[18]

The **TS6** (Table 2) describes a single hydrogen shift from C4 to O4, which is not much advanced, and a C3−O3 bond breaking and a double C3−C4 bond formation. The process is more synchronic than the preceding cases, and the transition structure has an intermediate character between reactants and products.

At **TS7** (Table 2), seven bonds participate in a one-step decomposition yielding the final products. However, some of them have not advanced at all (C1−C2 bond breaking) or have evolved to a very little extent (C2−O3 double bond formation to give formaldehyde). Then, a very asynchronous process is described with some breaking bond processes very advanced (C3−O3 and C4−H4), some bond formations halfway to their

final state (O1−H4 and C3−C4 double bond formation), and the aforementioned late evolutions of C1−C2 and C2−O3.

An analysis of the NBO charges at **TS1** shows an important positive charge developed on H1 (0.56 at TS, 0.40 at reactant, for **I** decomposition) and a very high positive charge on C1 (0.91 at TS, 0.76 at reactant, for the same model system), while the three oxygens support the electronic excess, having calculated charges −0.78 for O1, −0.75 for O2, and −0.79 for O3 at TS, and −0.62 for O1, −0.56 for O2, and −0.68 for O3 at reactant. Surprisingly, C2 does not support positive charge, having its calculated charge negative, −0.04, at **TS1**−**I** (slightly positive, 0.03, at reactant). Then, from an electronic point of view, the possible positive charge developed on C2 moves to C1, where it is highly stabilized by the negative charges on O1 and O2. A very similar analysis can be made for the **TS1** corresponding to the **II** and **III** systems.

Conclusions

The reaction pathways for the decomposition of methoxy, ethoxy, and isopropoxyacetic acids have been theoretically studied at the MP2/6-31G** level. The first-order rate coefficients for the decomposition processes were evaluated in terms of the TST. The theoretical results have been confronted with experimental data and the results can be summarized as follows.

(1) Five reaction pathways have been found for **II** and **III** systems on the PES, while for **I** system two reaction pathways are possible. Among these pathways, the reaction mechanism A was found to be favorable, via **TS1**; the first step of mechanism A can be considered as the rate-limiting step.

(2) The appearance of propene as a subproduct of the reaction can be explained by the presence of reaction pathways C and D on the PES associated with the isopropoxyacetic acid decomposition process.

(3) For all transition structures found, the main geometric parameters and fluctuations described by the transition vector are invariant to the system size.

(4) An analysis of bond orders suggests that the enlargement of the C2−O3 bond with initial migration of the H1 atom can be seen as the driving force for the decomposition process at **TS1**. The possible positive charge appearing at C2 moves to C1, where it is stabilized by the negative oxygens.

(5) The decomposition reactions can be described as asynchronous concerted processes, particularly the first step of the A reaction pathway.

(6) A comparison of the calculated and experimental kinetic parameters shows a quantitative agreement.

Acknowledgment. This work was supported by research funds of the Ministerio de Educación y Ciencia of the Spanish Government by DGICYT (Project PB96-0795-C02-02) and of the Universitat de València (Project UV97-2219). All calculations were performed on two Silicon Graphics Power Challenge L of the Servei d'Informàtica of the Universitat Jaume I. We are most indebted to this center for providing us with computer capabilities.

Supporting Information Available: Tables 1as−1es, including imaginary frecuency, Hessian unique negative eigenvalue, main components of the transition vector, and corresponding geometric parameters for **TS1**−**I**, **TS1**−**II**, **TS1**−**III**, **TS3**−**I**, **TS3**−**II**, **TS3**−**III**, **TS4**−**II**, **TS4**−**III**, **TS6**−**II**, **TS6**−**III**, **TS7**−**II**, and **TS7**−**III**. This material is available free of charge via the Internet at http://pubs.acs.org.

References and Notes

(1) Chuchani, G.; Rotinov, A.; Martín, I.; Avila, I.; Domínguez, R. M. *J. Phys. Chem.* **1985**, *89*, 4134.
(2) Domínguez, R. M.; Rotinov, A.; Chuchani, G. *J. Phys. Chem.* **1986**, *90*, 6277.
(3) Chuchani, G.; Martín, I.; Rotinov, A.; Domínguez, R. M.; Pérez, I. M. *J. Phys. Org. Chem.* **1995**, *8*, 133.
(4) Chuchani, G.; Rotinov, A.; Domínguez, R. M. *J. Phys. Org. Chem.* **1996**, *9*, 787.
(5) Chuchani, G.; Rotinov, A.; Domínguez, R. M.; Martín, I. *J. Phys. Org. Chem.* **1996**, *9*, 348.
(6) Williams, I. H. *Chem. Soc. Rev.* **1993**, 277.
(7) Skancke, P. N. *Acta Chem. Scand.* **1993**, *47*, 629.
(8) Glasstone, K. J.; Laidler, K. J.; Eyring, H. *The Theory of Rate Processes*; McGraw-Hill: New York, 1941.
(9) Laidler, K. J. *Theories of Chemical Reaction Rates*; McGraw-Hill: New York, 1969.
(10) Heidrich, D.; Kliesch, W.; Quapp, W. *Properties of Chemically Interesting Potential Energy Surfaces*; Springer-Verlag: New York, 1991.
(11) Marcus, R. A. *J. Chem. Phys.* **1965**, *43*, 1598.
(12) Forst, W. *Theory of Unimolecular Reactions*; Academic Press: New York, 1973.
(13) Truhlar, D. G.; Garrett, B. C. *Acc. Chem. Res.* **1980**, *13*, 440.
(14) Truhlar, D. G.; Isaacson, A. D.; Garrett, B. *Theory of Chemical Reaction Dynamics*; Chemical Rubber Co.: Boca Raton, FL, 1985.
(15) Tapia, O.; Andres, J. *J. Mol. Struct. (THEOCHEM)* **1995**, *335*, 267.
(16) Tapia, O.; Andrés, J.; Stamato, F. L. M. G. In *Solvent Effects and Chemical Reactivity*; Tapia, O.; Bertrán, J., Eds.; Kluwer Academic Publishers: Dordrecht, 1996; p 283.
(17) Safont, V. S.; Moliner, V.; Andrés, J.; Domingo, L. R. *J. Phys. Chem.* **1997**, *101*, 1859.
(18) Domingo, L. R.; Andrés, J.; Moliner, V.; Safont, V. S. *J. Am. Chem. Soc.* **1997**, *119*, 6415.
(19) Domingo, L. R.; Picher, M. T.; Andrés, J.; Safont, V. S.; Chuchani, G. *Chem. Phys. Lett.* **1997**, *274*, 422.
(20) Frisch, M. J.; Pople, J. A.; Binkley, J. S. *J. Chem. Phys.* **1984**, *80*, 3265.
(21) Frisch, M. J.; Trucks, G. W.; Schlegel, H. B.; Gill, P. M. W.; Johnson, B. G.; Robb, M. A.; Cheeseman, J. R.; Keith, T.; Peterson, G. A.; Montgomery, J. A.; Raghavachari, K.; Al-Laham, M. A.; Zakrzewski, V. G.; Ortiz, J. V.; Foresman, J. B.; Cioslowski, J.; Stefanov, B. B.; Nanayakkara, A.; Challacombe, M.; Peng, C. Y.; Ayala, P. Y.; Chen, W.; Wong, M. W.; Andres, J. L.; Replogle, E. S.; Gomperts, R.; Martin, R. L.; Fox, D. J.; Binkley, J. S.; Defrees, D. J.; Baker, J.; Stewart, J. P.; Head-Gordon, M.; Gonzalez, C.; Pople, J. A. *GAUSSIAN94*, Revision B.1; Gaussian, Inc.: Pittsburgh, PA, 1995.
(22) Schlegel, H. B. *J. Comput. Chem.* **1982**, *3*, 214.
(23) Schlegel, H. B. *J. Chem. Phys.* **1982**, *77*, 3676.
(24) McIver, J., Jr. W. *Acc. Chem. Res.* **1974**, *7*, 72.
(25) Fukui, K. *J. Phys. Chem.* **1970**, *74*, 4161.
(26) González, C.; Schlegel, H. B. *J. Phys. Chem.* **1990**, *94*, 5523.
(27) González, C.; Schlegel, H. B. *J. Chem. Phys.* **1991**, *95*, 5853.
(28) Hehre, W. J.; Radom, L.; Schleyer, P. v. R.; Pople, J. A. *Ab Initio Molecular Orbital Theory*; John Wiley & Sons: New York, 1986.
(29) McQuarrie, D. *Statistical Mechanics*; Harper & Row: New York, 1986.
(30) *GaussView 1.0*; Gaussian, Inc.: Pittsburgh, PA, 1997.
(31) Varandas, A. J. C.; Formosinho, S. J. F. *J. Chem. Soc., Faraday Trans. 2* **1986**, 282.
(32) Lendvay, G. *J. Mol. Struct. THEOCHEM* **1988**, *167*, 331.
(33) Lendvay, G. *J. Phys. Chem.* **1989**, *93*, 4422.
(34) Wiberg, K. B. *Tetrahedron* **1968**, *24*, 1083.
(35) Reed, A. E.; Curtiss, L. A.; Weinhold, F. *Chem. Rev.* **1988**, *88*, 899.
(36) Reed, A. E.; Weinstock, R. B.; Weinhold, F. J. *J. Chem. Phys.* **1985**, *83*, 735.
(37) Moyano, A.; Pericàs, M. A.; Valentí, A. *J. Org. Chem.* **1989**, *54*, 573.